Disentangling magnetic subfabrics and their link to deformation processes in cleaved sedimentary rocks from the Internal Sierras (west central Pyrenees, Spain)

B. Oliva-Urcia [a,*], J.C. Larrasoaña [b], E.L. Pueyo [c], A. Gil [d], P. Mata [e], J.M. Parés [a], A.M. Schleicher [a], O. Pueyo [d]

[a] Department of Geological Sciences, University of Michigan, 2534 CC. Little Building, Ann Arbor, MI 48109-1063, USA
[b] Institut de Ciències de la Terra Jaume Almera, CSIC, C/Solé i Sabarís s/n, 08028 Barcelona, Spain
[c] Instituto Geológico y Minero de España, Unidad de Geología y Geofísica, Oficina de Zaragoza, C/Manuel Lasala 44, 9°B, 50006 Zaragoza, Spain
[d] Universidad de Zaragoza, Dpto. Geodinámica Interna, C/Pedro Cerbuna 12. 50009 Zaragoza, Spain
[e] Facultad de Ciencias de Mar y Ambientales, Universidad de Cádiz, Campus de Puerto Real, 11510 Puerto Real, Cádiz, Spain

ARTICLE INFO

ABSTRACT

Here we present a detailed study of the magnetic fabrics and subfabrics of remagnetized Upper Cretaceous limolites that crop out in the Internal Sierras (west central Pyrenees) affected by a penetrative pressure-solution cleavage. The bulk magnetic fabrics of these rocks (RT-AMS) show variable orientations that do not conform to what is typically reported for cleaved sedimentary rocks. In contrast, the paramagnetic subfabrics (LT-AMS) show remarkably constant directional properties, so that their K_{max} and K_{min} axes cluster parallel to the intersection lineation and to the poles to bedding, respectively. These LT-AMS subfabrics indicate a preferred orientation of phyllosillicates that is consistent with a syn-sedimentary (Late Cretaceous) period of NNE-oriented layer-parallel shortening. Noticeably, these phyllosillicate subfabrics are not further altered by the subsequent formation of cleavage in the Late Eocene–Early Oligocene. The ferrimagnetic subfabrics (AARM) also show remarkably constant orientation, so that their K_{max} axes are strikingly parallel to the shortening direction in the area. We interpret this preferred orientation of ferrimagnetic grains as being caused by subhorizontal shear associated to cleavage formation, which is consistent with the age and mechanisms (authigenic growth and rotation of pre-existing magnetite grains) proposed for the pervasive remagnetization that affects the studied rocks.

© 2008 Elsevier Ltd. All rights reserved.

1. Introduction

Magnetic fabrics have been long used to decipher the tectonic evolution of fold and thrust belts during low-to-moderate deformation conditions. In particular, the evolution of magnetic fabrics from the external to the internal parts of orogenic belts, where a transition from weakly deformed to heavily cleaved rocks is typically observed, has been the focus of several studies (e.g. Borradaile and Tarling, 1981, 1984; Kissel et al., 1986; Averbuch et al., 1992; Parés and Dinarès-Turell, 1993; Sagnotti and Speranza, 1993; Parés et al., 1999; Larrasoaña et al., 2004). According to these studies, in the most external units of orogenic wedges, where deformation is very weak and restricted to syn-sedimentary layer-parallel shortening (LPS), tectonic deformation is able to overcome the initial sedimentary fabric and to reorient phyllosilicate grains according to the prevailing stress field. Thus, K_{max} axes tend to align perpendicular to the shortening direction whereas K_{min} axes remain parallel to the bedding plane. As deformation increases, development of pencil structures and weak cleavage modify the magnetic ellipsoid in such a way that K_{max} axes become tightly clustered parallel to fold axes and to the strike of thrust sheets, and K_{min} axes begin to develop a girdle parallel to the shortening direction. When cleavage is well-developed in response to increased deformation, the principal magnetic susceptibility directions parallel the flattening plane of the finite-strain ellipsoid, so that the K_{min} axes become perpendicular to tectonic foliation and the K_{max} axes parallel the elongation direction, which usually is the intersection of the bedding and cleavage planes (L_1) (Singh et al., 1975; Borradaile and Tarling, 1981; Kligfield et al., 1981; Hrouda, 1982; Borradaile, 1987; Aubourg et al., 1995; Borradaile and Henry, 1997; Parés et al., 1999; Aubourg et al., 2000; Parés and van der Pluijm, 2002). Further deformation might result in the re-alignment of K_{max} axes producing an obliquity of K_{max} respect to the structural foliation (Rathore, 1985; Aranguren et al., 1996; Borradaile et al., 1998), so that the angular deviation provides a sense of shear. In some occasions, K_{max} axes are found parallel to the transport direction of thrust sheets, while K_{min} axes remain clustered perpendicular to foliation (Averbuch et al., 1992; Aubourg et al., 1999).

The anisotropy of magnetic susceptibility of rocks is typically measured at room temperature (RT-AMS), so that it results from the bulk contribution of all rock-forming minerals regardless of their magnetic behavior (Hrouda, 1982; Kelso et al., 2002; Martín-Hernández and Ferré, 2007). Since different minerals might form at different times and under different conditions, and might respond differently to tectonic deformation, separating their individual subfabrics is important for unraveling the geological history of rocks from its formation through their subsequent tectonic evolution (Borradaile and Henry, 1997; Aubourg et al., 1991, 2000; Robion et al., 1999; Aubourg and Robion, 2002; Kelso et al., 2002; Martín-Hernández and Ferré, 2007). Of particular importance in tectonic studies has been the separation of complex RT-AMS fabrics into meaningful paramagnetic and ferromagnetic subfabrics that have contributed to disentangle the tectonic evolution of orogenic wedges (Borradaile and Jackson, 2004).

Here we present the first detailed study of composite magnetic fabrics of remagnetized Upper Cretaceous sedimentary rocks from the Internal Sierras (Oliva-Urcia and Pueyo, 2007; Oliva-Urcia et al., 2008), which crop out within a domain of pressure-solution cleavage developed during the Tertiary compression in the internal part of the west central Pyrenees (Choukroune, 1976). Separation of the bulk magnetic fabrics into their paramagnetic and ferrimagnetic subfabrics, which has been based on magnetic methods and on mineralogical techniques, has made possible the unraveling of complex RT-AMS fabrics that do not show a common pattern with respect to tectonic elements. This, together with structural and paleomagnetic data available for the studied area, has enabled a more detailed determination of the deformational history of the Internal Sierras in the context of the Pyrenean orogeny.

## 2. Geological setting and sampling

The Pyrenean orogen is an asymmetric mountain belt formed between the Eurasian and Iberian plates during Cretaceous to Miocene times (Muñoz, 1992). The southern part of the west central Pyrenees is characterized by a set of south verging, imbricated thrust sheets that developed in a piggyback fashion as deformation progressed towards the foreland (Teixell, 1996, 1998) (Fig. 1). The northernmost of these units, the Lakora thrust, evolved from Late Cretaceous (Santonian) to Middle Eocene (Bartonian) times involving cover and basement rocks (Séguret, 1972; Labaume et al., 1985; Teixell, 1992, 1996). Further to the south is the Larra-Monte Perdido cover thrust system, which formed during Middle Eocene (Lutetian–Bartonian) as a footwall splay of the Lakora basement thrust (Labaume et al., 1985; Teixell, 1992, 1996, 1998). Further deformation between the Late Eocene and the Early Oligocene (Priabonian–Rupelian) caused the southward emplacement of the underlying Gavarnie basement thrust sheet and resulted in an episode of major folding and increased tectonic loading (Teixell, 1992, 1996). This led to formation of a pressure-solution cleavage domain, with a fan-shaped geometry in the Axial Zone, the Internal Sierras, and the northern part of the Jaca-Pamplona basin (Fig. 1) (Choukroune, 1976). The temporal and geometrical relationships between cleavage and folding suggest that the cleavage formed during the latest stages of emplacement of the Gavarnie thrust sheet, likely from Late Eocene onwards (Choukroune and Séguret, 1973; Choukroune, 1976; Labaume et al., 1985; Teixell, 1992; Holl and Anastasio, 1995). Subsequent deformation active till the earliest Miocene (Aquitanian) moved the Guarga thrust sheet to the south, affecting the overlying thrust sheets, and exhumed the internal portions of the orogen (Labaume et al., 1985; Teixell, 1992, 1996).

The studied area is located at the western part of the Internal Sierras, a major topographic feature that bounds the Pyrenean Axial

Zone to the south (Fig. 1). The Internal Sierras are make up of Mesozoic–Tertiary rocks, which are affected by the Larra-Monte Perdido thrust system. This system has 3–5 km of displacement to the south and a N200 (Séguret, 1972) or SW transport direction (Teixell et al., 2000) in the studied sector of the Internal Sierras. We have focused our sampling on Campanian to Maastrichtian limolites from the Zuriza Marls and Marboré Sandstones formations, that were deposited during the Upper Cretaceous in the Iberian margin of the former Pyrenean rift (Séguret, 1972; Teixell, 1992; Martín-Chivelet et al., 2002). These rocks display a slaty cleavage with anastomosing cleavage planes that have a strong fissility (>10 for the Zuriza Marls Fm. in the scale of Durney and Kisch, 1994; see Teixell et al., 2000) (Fig. 2). In the studied area, cleavage planes strike E–ESE, dip moderately to the North, and often have a down dip stretching lineation, which indicates that the cleavage has a ductile behavior and has undergone shear deformation (Teixell et al., 2000). Calculation of burial depths from balancing cross-section indicates that the Upper Cretaceous rocks reached a temperature of 200 °C (Teixell et al., 2000), which is consistent with the 250 °C estimated from chemical analysis of fluid inclusions in veins (Travé et al., 1997; McCaig et al., 2000) and the 300 °C deduced from vitrinite reflectance data (Teixell et al., 2000). There is evidence for an earlier layer-parallel shortening in the area (Teixell et al., 2000).

Extensive paleomagnetic results from the Internal Sierras indicate that limolites from the Zuriza and Marboré formations are affected by a pervasive remagnetization that is carried by magnetite, has a systematic reverse polarity, and was acquired after folding and after the emplacement of the Gavarnie basement thrust (Oliva-Urcia and Pueyo, 2007; Oliva-Urcia et al., 2008). In many cases (i.e. 30% of the studied sites), a primary prefolding magnetization also carried by magnetite is preserved in these rocks. The remagnetization has been related to the development of the cleavage domain in the Internal Sierras during the latest Eocene (Oliva-Urcia and Pueyo, 2007), which is consistent with the Middle–Late Eocene age of the youngest sediments affected by cleavage in the area (turbidites from the Hecho group; Labaume et al., 1985; Teixell, 1996). The presumed mechanism for explaining the remagnetization event is the liberation and reorientation of previously existing magnetite grains during formation of pressure-solution cleavage planes, although dissolution of pre-existing magnetite grains and precipitation of new magnetic phases (Suk et al., 1990, 1993; Housen et al., 1993a; Lewchuk et al., 2003; Zegers et al., 2003; Evans and Elmore, 2006) cannot be excluded (Oliva-Urcia et al., 2008).

We have collected nine sites from Upper Cretaceous belonging to the Zuriza Marls Fm. (sites 4–8) and Marboré Sandstones Fm. (sites 1–3 and 9), in the western sector of the Internal Sierras. At every site, 10 standard paleomagnetic cores were drilled with a portable, water-refrigerated drill machine. These sites were selected because: (1) they are located in a very similar structural setting, near the floor thrust of the Larra-Monte Perdido system and affected by the pressure-solution cleavage; and (2) they display different angular relationships between bedding and cleavage, which might help to enhance any genetic link between magnetic fabrics and deformation. Sites 1–3 come from an outcrop where an excellent example of cleavage refraction is observed affecting the limolites from the Marboré Sandstone Fm. Sites 5 and 6 were drilled in the Zuriza Marls Fm. located in the northern limb of a gentle, metric-scale hangingwall anticline. Sites 7 and 8, also drilled in the Zuriza Marls Fm., are located in the northern limb of a decametric anticline, and site 9, coming from an outcrop of the Marboré Sandstones Fm., is located in the southern limb of the same structure. Site 4 was drilled in limolites from the Zuriza Marls Fm., in the only outcrop where a stretching lineation, subvertical in attitude, has been found in the field.
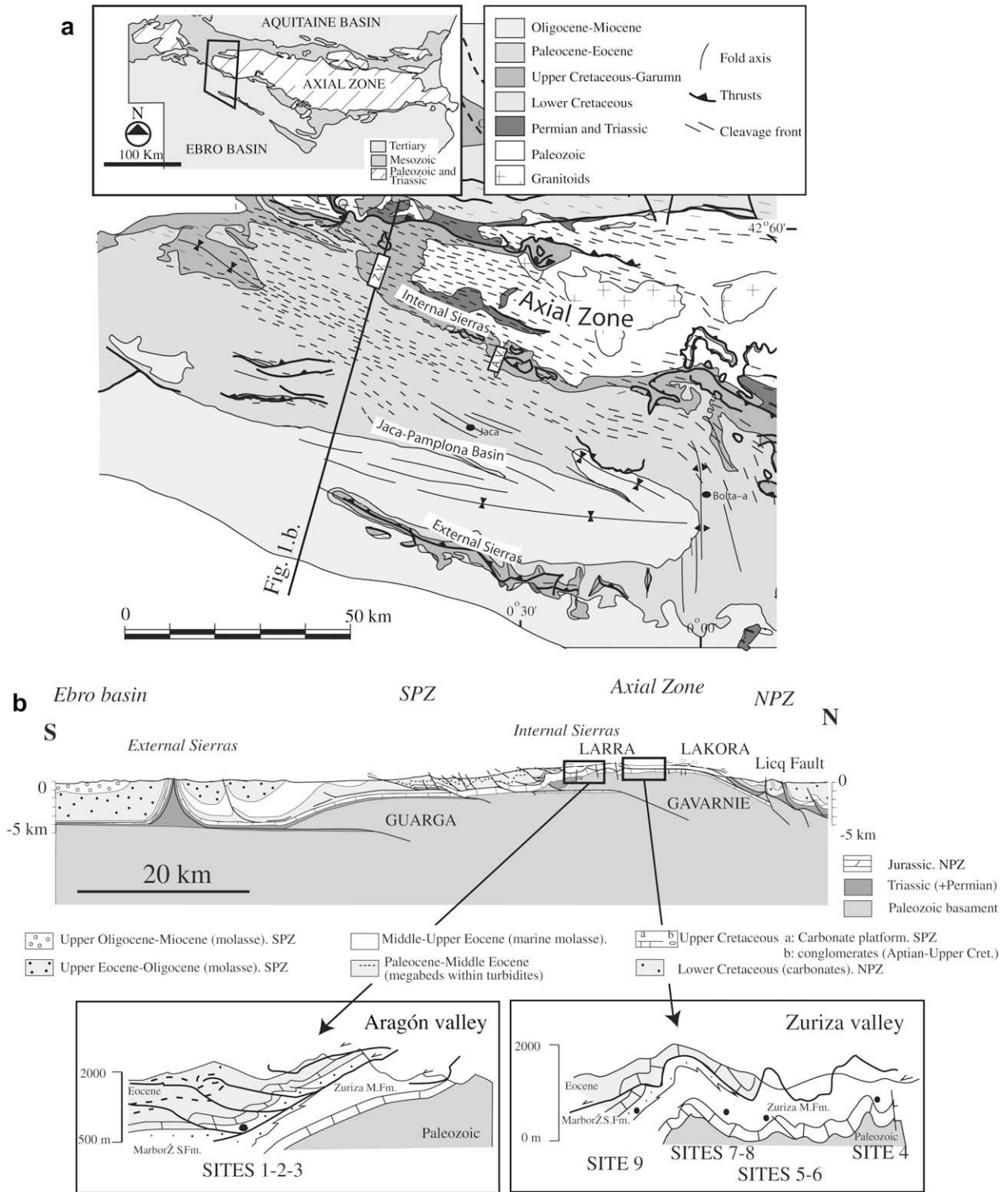
Fig. 1. (a) Geological map of the west central Pyrenees, with location of the Zuriza and Aragón valleys. (b) Cross-section along the western part of the central Pyrenees (modified from Teixell, 1996, 1998; Millán, 1996). SPZ and NPZ denote the South and North Pyrenean Zones, respectively.

3. Methods

RT-AMS analyses, to which all minerals contribute, were performed in the laboratory of magnetic fabrics of the University of Zaragoza. Between 25 and 40 specimens per site were measured using a KLY3 Kappabridge (AGICO). The AMS is a second-rank tensor that can be graphically displayed by a three-axes ellipsoid ($K_{max} > K_{int} > K_{min}$) with a given direction, shape and degree of anisotropy. We have used the eigenvectors of the susceptibility axes to determine the orientation of the magnetic ellipsoid. Their shapes have been determined using the shape parameter T, whereas their degree of anisotropy have been established using the corrected anisotropy degree P' (Jelínek, 1981). We have also used other parameters, such as the magnetic lineation ($L = K_{max}/K_{int}$) and foliation ($F = K_{int}/K_{min}$), to better characterize the magnetic ellipsoids. In addition to these parameters, we have also used the bulk
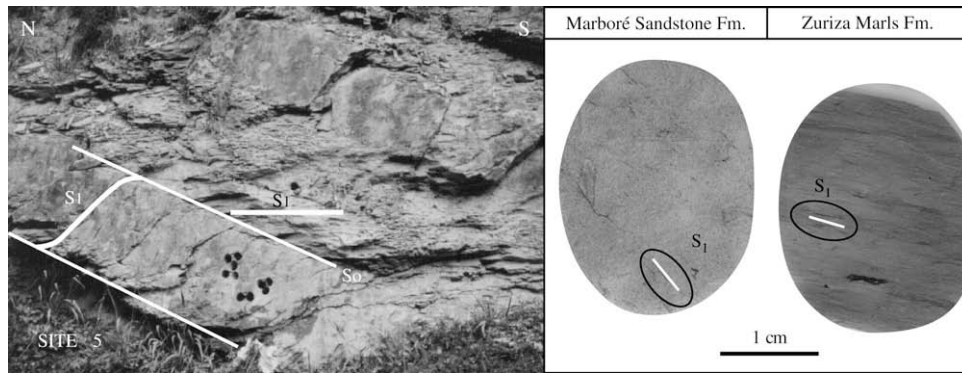
Fig. 2. Field (left) and thin section (right) aspect of cleavage planes developed in the studied area.

susceptibility $K_m = K_{max} + K_{int} + K_{min}/3$ to represent the mean value of the integral of the directional susceptibilities over the whole rock-specimen (Nagata, 1961).

Low-temperature AMS (LT-AMS) analyses were done in the paleomagnetic laboratory of the University of Michigan. The LT-AMS was analyzed in 3–6 samples per site using a SI2B susceptibility meter with an internal coil frequency of 19.2 kHz (Sapphire Instruments). Samples were immersed in liquid nitrogen (77 K for 30 min) before the magnetic susceptibility was measured along six different axes. The magnetic susceptibility of paramagnetic minerals (i.e. mainly phyllosilicates) is enhanced at low temperatures following the Curie–Weiss law (see Parés and van der Pluijm, 2002 for more details), so that at nitrogen temperatures the K_{max} axes increase by a factor larger than the K_{min}. This produces a magnetic susceptibility intensity 3–5 times higher than at room temperature (Parés and van der Pluijm, 2002), which mainly reflects the subfabric associated to paramagnetic minerals.

In order to better determine the paramagnetic subfabric residing in phyllosilicates, we have performed high-resolution X-ray texture goniometry analyses (XTG, van der Pluijm et al., 1994) to determine the crystallographic preferred orientation of phyllosilicates in very small regions (1 mm). We have used an Enraf-Nonious CAD4 automated single-crystal diffractometer housed in the EMAL laboratory at the University of Michigan, which is equipped with a molybdenum source and allows measurement to be taken in the transmission mode. The preferred orientation data of the phyllosilicates were determined using the (001) basal plane reflection (d:10 Å for mica and d:7 Å for chlorite). The normalized intensity data are expressed in multiples of random distribution (m.r.d., Wenk, 1985), which provide an indication on the alignment of the phyllosilicate layers.

The Anisotropy of the Anhysteretic Remanence Magnetization (AARM) was analyzed for 5–9 specimens per site using a SI-4 AF demagnetizer (Sapphire Instruments). Samples were subjected to an AF demagnetizing peak field of 100 mT while a 0.05 mT direct field was applied in a window of 5–60 mT. The window was chosen after partial Anhysteretic Remanent Magnetization measurements (pARM), and corresponds to the window range containing the highest pARM (Jackson et al., 1988). This procedure was performed in nine different axes for every sample, measuring the remanent magnetization for every position in a 2G-cryogenic magnetometer. After each measurement, the sample was demagnetized along three orthogonal directions with an AF peak field of 100 mT. The computation of the AARM ellipsoid, which enables identification of the ferrimagnetic subfabric, was done using the Magnetic Anisotropy Analyses 3.1 (ARMA.exe; McCabe et al., 1985). The anisotropy tensor was calculated by the least-squares method (Girdler, 1961).

We have also used mineralogical and rock magnetic techniques in order to identify the paramagnetic and ferromagnetic minerals present in the studied rocks. A scanning electron microscopy (SEM)

study of selected samples was conducted in order to examine the composition of paramagnetic and ferromagnetic minerals and their textural relationship with cleavage planes. Selected polished samples were cut perpendicular to the cleavage plane and parallel to its dip direction, and were coated with carbon. Backscattered imaging and semiquantitative analyses of the mineral composition have been obtained using two SEM/EDX systems in the EMAL laboratory (SEM Hitachi S3200N; 20 kV, BSE detector, EDX analyses) and the University of Cádiz (ESEM quanta FEI, 20 kV, BSE detector, EDX analyses, Phoenix system). Due to their very low concentrations, ferromagnetic minerals were better identified by applying rock magnetic techniques, such as: (1) thermal demagnetization of a composite IRM (Lowrie, 1990); (2) low-temperature experiments (Weil and van der Voo, 2002); and (3) hysteresis loops (Parry, 1982). The first type of experiments were performed on standard paleomagnetic cores with a Walker electromagnet, an ASC Scientific thermal demagnetizer, and a three-axis 2G Enterprises cryogenic magnetometer housed at the paleomagnetic laboratory of the University of Michigan. Low-temperature experiments and hysteresis loops were performed on rock and rock-powder chips at the Institute for Rock Magnetism (University of Minnesota, USA) using a MPMS magnetometer (Quantum Design Ltd.), a Micro VS Magnetometer (Princeton Instrument Corporation), and a Vibrating Sample Magnetometer (Princeton I.C.).

4. Results

4.1. RT-AMS

Bulk susceptibility values (K_m) range between 153 and 290 (10^{-6} SI) (Fig. 3a, Table 1), which is typical for rocks where the paramagnetic minerals are the main contributors (Rochette, 1987), although the K_m value is not diagnostic of the RT-AMS carrier (Hirt et al., 2004). The bulk susceptibility shows a relatively narrow range for the corresponding corrected anisotropy degree values (P'), which range between 1.01 and 1.09, regardless of lithology (Fig. 3a and Table 1). The K_{max} axes for all sites appear to be well clustered (Fig. 4, Table 1 in supplementary material). It is noticeable that the RT-AMS magnetic ellipsoids display distinctly different directional properties although all sites are located in a very homogeneous structural context. Thus, K_{min} axes are perpendicular to bedding in most sites (1 and 4–8), but they appear located away from the pole to bedding in other cases (sites 2, 3, 9). The K_{max} axes are roughly parallel to the intersection lineation in sites (5, 6, 9), but they are either perpendicular to it (sites 2–4) or at some intermediate position (sites 1, 7, 8) (Fig. 4). Perhaps the most remarkable fact is that none of the RT-AMS ellipsoids conform to that typically observed in cleaved rocks, where K_{max} and K_{min} axes appear clustered around the intersection lineation and the pole to cleavage, respectively (Singh et al., 1975; Borradaile and Tarling,
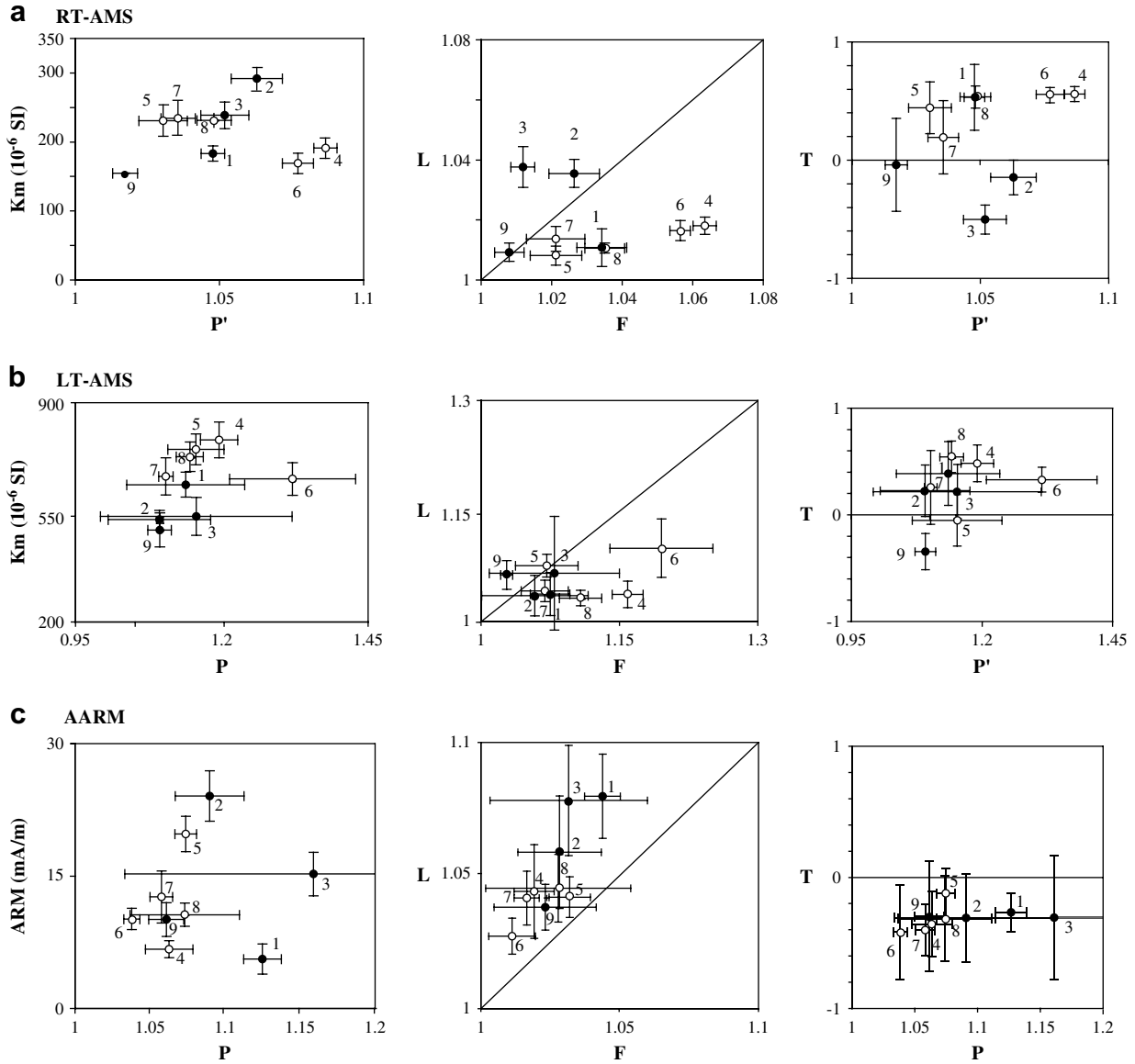
Fig. 3. Bi-plots showing the relationship between different parameters that characterize the RT-AMS (a), LT-AMS (b) and AARM (c) ellipsoids. Numbers indicate the site. Black and white circles denote sites drilled in limolites of the Marboré Sandstone and Zuriza Marls formations, respectively.

1981; Hrouda, 1982; Borradaile, 1987; Housen and van der Pluijm, 1991; Aubourg et al., 1995, 2000; Borradaile and Henry, 1997; Parés et al., 1999; Parés and van der Pluijm, 2002). Actually, K_{min} axes cluster around the pole to cleavage only when this is parallel to bedding (sites 4, 6), and cluster closer to the pole to bedding when they are not parallel (sites 5, 7, 8). In the only site where stretching lineations have been found, they are parallel to K_{max} axes (site 4) as expected (Fig. 4).

4.2. LT-AMS

Site-mean values of the magnetic susceptibility at low-temperature range between 491 and 788 (10^{-6} SI), and tend to be lower for limolites of the Marboré Sandstones Formation (Fig. 3b, Table 1). The bulk susceptibility at low temperature is between 1.8 and 4 times larger than at room temperature. The ratio K_{LT}/K_{RT} is a proxy for the content of paramagnetic grains, mostly phyllosilicates, in the studied rocks. This value is lower for sites 2 and 3 and higher for sites 4 and 6, which indicates relatively lower and higher

concentration of phyllosilicates, respectively (Fig. 5a). With the exception of sites 2 and 3, the phyllosilicate content is directly related to the corrected anisotropy degree at room temperature (Fig. 5b). With regard to the directional properties of the LT-AMS ellipsoids, and regardless of the limited amount of data available, it is remarkable that they show a much more homogeneous behavior compared to the RT-AMS ellipsoids (Fig. 4). Thus, K_{max} axes have a W–NW orientation, broadly parallel to the intersection lineation, in all cases except at site 4, where K_{max} axes are perpendicular to the intersection lineation and subparallel to the stretching lineation. Similarly, K_{min} axes are broadly perpendicular to bedding, but not to cleavage, with the exception of site 9, where they appear to lie in an intermediate position between the poles to bedding and cleavage (Fig. 4). Noticeably, the LT-AMS ellipsoids partly conform the typical orientation of the AMS ellipsoid observed in cleaved rocks, where K_{max} axes appear clustered around the intersection lineation (Lamarche and Rochette, 1987; Borradaile and Tarling, 1981; Hrouda, 1982; Borradaile, 1987; Housen and van der Pluijm, 1991; Aubourg et al., 1995; Borradaile and Henry, 1997; Parés et al., 1999;

Table 1
Site-mean parameters characterizing the RT-AMS (upper panel), LT-AMS (middle panel), and AARM (lower panel).

Site	K_{mean} ($\times 10^{-6}$)	L	F	P'	T	K_{max} (D&I)	K_{int} (D&I)	K_{min} (D&I)
RT-AMS								
NAT1	182.39	1.011	1.034	1.048	0.526	220.09	310.05	71.80
NAT2	290.79	1.035	1.027	1.063	−0.151	30.09	280.66	125.22
NAT3	237.68	1.037	1.012	1.052	−0.508	33.05	297.43	129.46
NAT4	190.06	1.018	1.064	1.087	0.554	81.71	291.16	199.09
NAT5	229.93	1.008	1.021	1.031	0.438	291.14	197.19	56.67
NAT6	168.09	1.016	1.057	1.077	0.553	284.13	190.12	63.72
NAT7	233.19	1.014	1.021	1.036	0.188	59.21	321.18	196.62
NAT8	230.31	1.010	1.035	1.048	0.530	73.17	335.25	194.60
NAT9	153.74	1.009	1.008	1.018	−0.045	266.02	175.56	353.33
LT-AMS								
NAT1	636.193	1.036	1.076	1.136	0.382	282.15	185.23	36.65
NAT2	524.866	1.034	1.059	1.092	0.221	327.12	229.29	80.64
NAT3	534.950	1.065	1.080	1.154	0.213	314.12	238.13	102.77
NAT4	779.090	1.036	1.160	1.192	0.478	101.47	302.41	203.10
NAT5	748.517	1.075	1.072	1.153	−0.056	304.02	214.28	37.63
NAT6	654.194	1.099	1.196	1.315	0.325	310.01	215.26	44.64
NAT7	662.854	1.041	1.070	1.103	0.252	308.18	45.21	184.60
NAT8	725.350	1.031	1.109	1.143	0.538	307.14	43.28	192.55
NAT9	491.408	1.062	1.028	1.092	−0.349	302.05	38.36	210.54

Site	mA/m	L	F	P	T	K_{max} (D&I)	K_{int} (D&I)	K_{min} (D&I)
AARM								
NAT1	4.843	1.080	1.044	1.127	−0.271	25.04	295.17	129.78
NAT2	23.981	23.981	1.059	1.089	−0.304	37.13	235.75	320.08
NAT3	15.164	15.164	1.078	1.161	−0.311	28.03	300.24	07.76
NAT4	6.639	6.639	1.044	1.064	−0.361	67.81	225.06	317.04
NAT5	19.695	19.695	1.042	1.075	−0.127	196.26	5.64	105.03
NAT6	10.065	10.065	1.027	1.039	−0.423	217.29	119.09	6.65
NAT7	12.554	12.554	1.041	1.059	−0.406	53.20	144.06	252.67
NAT8	10.532	10.532	1.045	1.075	−0.319	74.14	342.04	248.77
NAT9	10.007	10.007	1.038	1.062	−0.303	212.22	70.64	307.09

K_{mean} and AARM: susceptibility and ARM intensity; L: magnetic lineation; F: magnetic foliation; P': corrected anisotropy degree; P: anisotropy degree; T: shape factor; K_{max}, K_{int}, K_{min}: direction and plunge of the maximum, intermediate and minimum susceptibility axes.

Aubourg et al., 2000; Ferré and Améglio, 2000; Hirt et al., 2000; Parés and van der Pluijm, 2002). On the contrary, the clustering of K_{min} around the bedding pole does not conform its typical orientation in cleaved rocks (Housen et al., 1993b; Parés et al., 1999).

4.3. AARM

The intensity of the AARM varies between ca. 5 and 24 mA/m (Fig. 3c), and provides a proxy for the concentration of ferrimagnetic grains, whose concentration seems to be independent on lithology. In contrast to the predominant oblate shape of the RT-AMS and LT-AMS ellipsoids, T values for the AARM indicate a dominant prolate shape in all sites (Fig. 3c, Table 1). This prolate shape is typical for magnetite grains with a grain size larger than that of single domain particles (Borradaile et al., 1999; Aubourg et al., 2000), whereas smaller particles show more isotropic and oblate shapes (Sun et al., 1993). AARM ellipsoids display a remarkable homogeneity with regard to their directional properties (Fig. 4). Thus, K_{max} axes are broadly perpendicular to the intersection lineation (L_1) in all cases except in site 8, where the angle between the site-mean K_{max} and L_1 is around 30°. Moreover, site-mean K_{max} appear subhorizontal along a NNE or SSW direction, but in the case of site 4, where it is vertical. K_{min} axes tend to lie either around the bedding pole (site 7) or closer to the bedding pole than to the cleavage pole (sites 1, 8). In other cases, K_{min} form a girdle with K_{int} (sites 2, 3, 6 and 9) or appear parallel to L_1 (sites 4 and 5).

4.4. SEM observations

BSE images and XRD measurements of selected samples indicate that limolites are make up of grains that range between 50 and 100 μm in size (Fig. 6). The most abundant detrital minerals are quartz, calcite and phyllosilicates such as muscovite, chlorite and intergrowths of chlorite-mica. Calcite, albite, barite, and pyrite have been identified as the main authigenic minerals with variable concentrations. The main accessory minerals are monacite, zircons, apatite and Ti-oxides.

The phyllosilicates that are the main carriers of the LT-AMS are basically micas and Interleaved Phyllosilicate Grains (IPG) composed mainly by chorite/mica. IPG are the result of the stacking of thin (angstroms to microns) layers of phyllosilicates on (001) planes. The shape of the IPG in the studied samples varies from undeformed and tabular, deformed and tabular, to fussiform (Fig. 6b–e). The tabular shapes show rounded borders (Fig. 6c). Some IPG consist of one core crystal composed by mica (mainly muscovite), which can be up to 100 mm long, <20 mm thick, and is surrounded by chlorite flakes (Fig. 6b). Other intergrowths show shorter and more tabular or rhomboidal shapes composed by a larger number of layers, and are around 50 mm long and 20 mm thick (Fig. 6c and e). The IPG tend to lie parallel to bedding and oblique to cleavage planes (Fig. 6c), although in some cases they appear rotated or bent near cleavage planes (Fig. 6b, c and e). The presence of needles and grains of Ti-oxide may indicate the alteration of biotite or white mica rich in Ti (Veblen and Ferry, 1983) (Fig. 6a and b). In some cases we have observed very long, euhedral white mica crystals parallel to cleavage planes, which indicates authigenic formation during deformation (Fig. 6d).

Opaque iron-bearing minerals include pyrite and iron oxides (Fig. 6f–k). Whereas framboidal and euhedral pyrite is ubiquitous in all the studied samples (Fig. 6f–h), iron oxides have been observed only in two sites. At site 1, they appear as rounded masses of 5 μm located near cleavage planes (Fig. 6i). At site 2, they appear replacing either individual pyrite crystal in the outer part of pyrite framboids or euhedral, isolated pyrite crystal (Fig. 6j and k).
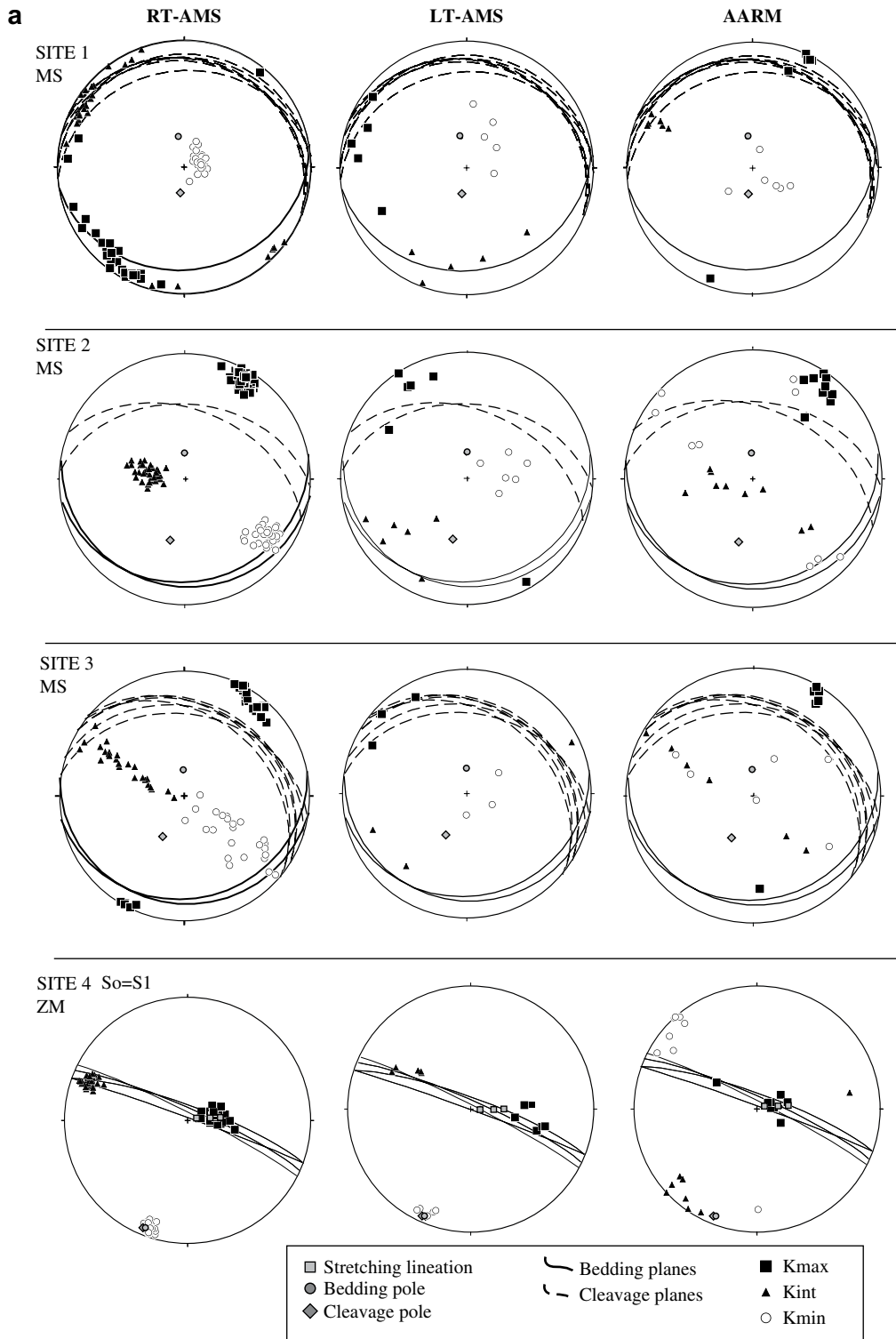
Fig. 4. Stereonet projections (lower hemisphere, equal area) of the RT-AMS (left), LT-AMS (middle) and AARM (right) susceptibility axes for each site, which are plotted along with the corresponding bedding and structural data. MS and ZM denote sites drilled in limolites of the Marboré Sandstone and Zuriza Marls formations, respectively.

4.5. High-resolution X-ray texture goniometry

The strength of the phyllosilicate layers stacking changes from site to site and also between the mica and chlorite crystals (Fig. 7). Overall, the mica crystals have a stronger fabric than chlorite, except for sites 4, 5 and 6, where m.r.d values for both minerals are very similar (Fig. 7). The strongest fabric associated with micas corresponds to site 4 (m.r.d. = 6.65), which shows exceptionally long crystals along cleavage planes indicating an authigenic origin linked to the formation of cleavage. The other sites show similarly strong preferred orientations of the mica crystals, with m.r.d. ranging between 2.9 and 3.8. The strongest fabric associated with chlorite is also observed in site 4 (m.r.d. = 6.93), having the other localities similarly strong preferred orientations of chlorite
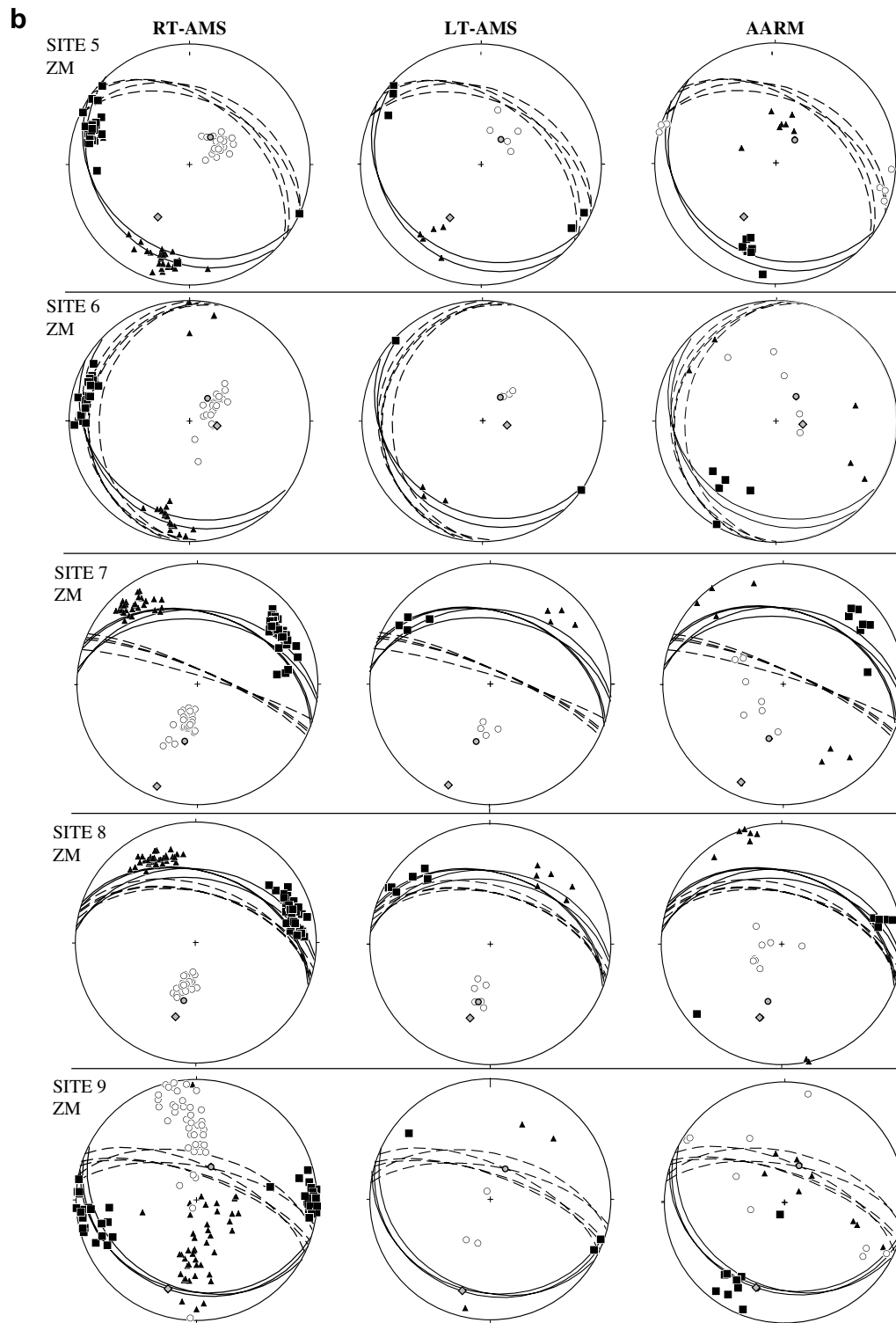
Fig. 4. (*continued*).

(m.r.d between 2.41 and 4.21). Overall, these values are similar to that found in other mudstones affected by cleavage (Ho et al., 1994).

4.6. Rock magnetism

Thermal demagnetization of the composite IRM indicates that magnetite is the main magnetic mineral in the studied samples (Fig. 8a). The presence of magnetite is confirmed by a marked Verwey transition observed at 120 K, which is present in most of the studied samples (Fig. 8b). Partial ARM (pARM) curves are very similar for all the studied samples (Fig. 8c), which indicates that magnetite has a grain size in the range of 5 μm (Jackson et al., 1988). Hysteresis loops, which are characterized by wasp-waited shapes, fall within the trend described for remagnetized limestones
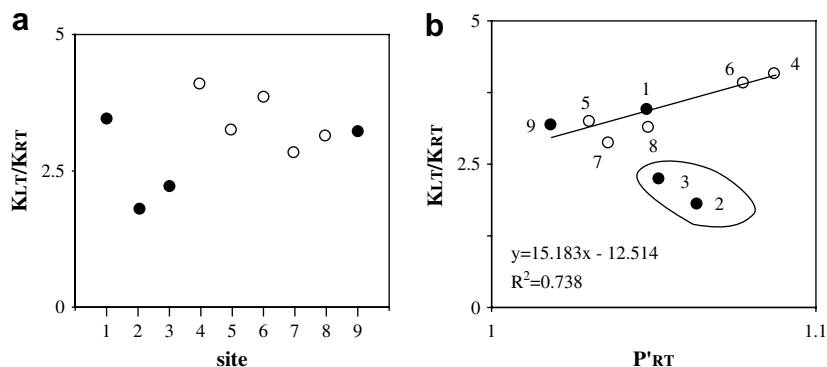
Fig. 5. (a) Plots showing the ratio between the intensity of the susceptibility at low (K_{LT}) and room (K_{RT}) temperatures for each site. (b) Plots showing the link between K_{LT}/K_{RT} ratios and P' at room temperature. Black and white circles denote sites drilled in limolites of the Marboré Sandstone and Zuriza Marls formations, respectively.

(Channell and McCabe, 1994) in the Day diagram (Fig. 8d) (Day et al., 1977), which is consistent with the presence of a pervasive remagnetization (Oliva-Urcia and Pueyo, 2007; Oliva-Urcia et al., 2008).

5. Discussion

5.1. Significance of the RT-AMS, LT-AMS and AARM

One of the most remarkable findings of our study is that, despite of the homogeneous structural setting and lithology considered, the RT-AMS ellipsoids do not show a homogeneous behavior. Another remarkable finding is that none of the RT-AMS ellipsoids conform to that typically observed in cleaved rocks. Thus K_{max} and K_{min} axes do not simultaneously cluster around the intersection lineation and the pole to cleavage, respectively, as it typically occurs in sedimentary rocks affected by cleavage (Singh et al., 1975; Borradaile and Tarling, 1981; Kligfield et al., 1981; Hrouda, 1982; Borradaile, 1987; Housen and van der Pluijm, 1991; Aubourg et al., 1995, 2000; Borradaile and Henry, 1997; Parés et al., 1999; Parés and van der Pluijm, 2002). Actually, K_{min} axes cluster around the pole to cleavage only when this is parallel to bedding (sites 4, 6), and cluster closer to the pole to bedding when they are not parallel (sites 5, 7, 8).

Application of the LT-AMS and AARM techniques enables the separation of these complex RT-AMS fabrics into mutually consistent phyllosilicate and ferrimagnetic subfabrics that display different directional properties. The studied sites can be divided into two main groups depending on the directional properties of their magnetic fabric and subfabrics. The first group (Type 1) includes those sites (4–6) where the orientation of the RT-AMS ellipsoid coincides with that of the LT-AMS but is different from that of the AARM. For sites belonging to this group, K_{min} axes of both the RT-AMS and LT-AMS cluster perpendicular to the bedding plane, but are often included within bedding in the case of the AARM. For both the RT-AMS and LT-AMS, K_{max} axes are parallel to the intersection lineation but in site 4, where they are parallel to the subvertical stretching lineation measured in the field. On the contrary, K_{max} axes of the AARM are perpendicular to the intersection lineation. Noticeably, Type 1 sites are characterized by the highest chlorite m.r.d. values. The second group (Type 2) includes those sites (1–3 and 7–9) where the orientation of the RT-AMS ellipsoid broadly coincides with that of the AARM but is different from that of the LT-AMS. Thus, K_{max} axes of both the RT-AMS and AARM are typically perpendicular to the intersection lineation, whereas those of the LT-AMS are parallel to it. Moreover, the orientation of the K_{min} and K_{int} axes of the RT-AMS is often similar

to their orientation in the case of the AARM, but less so to the case of the LT-AMS.

Based on these results, the similarity between the RT-AMS and the LT-AMS in Type 1 sites suggests that the phyllosilicates carrying the LT-AMS are also the main contributors to the RT-AMS. This might be due to an overwhelming contribution of chlorite, which reaches highest m.r.d. in Type 1 sites (Fig. 7). To the contrary, the similarity between the RT-AMS and the AARM in Type 2 sites suggests that the ferrimagnetic minerals carrying the AARM dominate the RT-AMS. Somehow surprisingly, there seems to be no link between this behavior and the concentration of ferrimagnetic minerals, as indicated by the similar ARM intensities for both Type 1 and 2 sites (Table 1). In other cases, the balanced competition between the AARM and LT-AMS ellipsoids might result in intermediate directions of the RT-AMS observed in some cases (e.g. sites 7 and 8). Noticeably, the K_{mean} value of Type 1 and 2 sites is remarkably similar and always less than 300×10^{-6} SI. These results suggest that: (1) caution must be taken when assessing the relative contribution of paramagnetic and magnetic minerals to the RT-AMS based only on mean K_{mean} values (Hirt et al., 2004); and (2) systematic separation of bulk magnetic fabrics into their paramagnetic and ferrimagnetic subfabrics is likely to provide additional insights in magnetic fabric studies even when the contribution of ferromagnetic grains is considered to be minor.

5.2. Tectonic and paleomagnetic implications

To the contrary of RT-AMS, and regardless of fabric type, LT-AMS ellipsoids display a homogeneous behavior with respect to structural elements (Fig. 4). Thus, their K_{max} axes cluster perpendicular to the shortening direction, and their K_{min} axes cluster around the bedding pole. Noticeably, this pattern does not conform to that typical observed for cleaved rocks, where K_{min} axes cluster parallel to the cleavage pole (Borradaile and Tarling, 1981; Hrouda, 1982; Borradaile, 1987; Housen and van der Pluijm, 1991; Aubourg et al., 1995, 2000; Borradaile and Henry, 1997; Parés et al., 1999; Parés and van der Pluijm, 2002). Instead, the orientation of the LT-AMS ellipsoids is identical to that typically found for weakly deformed mudrocks affected by layer-parallel shortening (Kissel et al., 1986; Aubourg et al., 1997; Parés et al., 1999; Parés and van der Pluijm, 2002; Larrasoaña et al., 2004). The magnetic fabric of such weakly deformed mudrocks is blocked during the earliest diagenesis, when the sediments are still unconsolidated, flat-lying, and the presence of water allows particulate rotation by intergranular slip and kinking (Parés et al., 1999; Larrasoaña et al., 2004). Under these conditions, layer-parallel shortening is able to overcome the initial sedimentary fabric (Fig. 9a) and to reorient phyllosilicate grains under the prevailing stress field, so that their K_{max} axes cluster
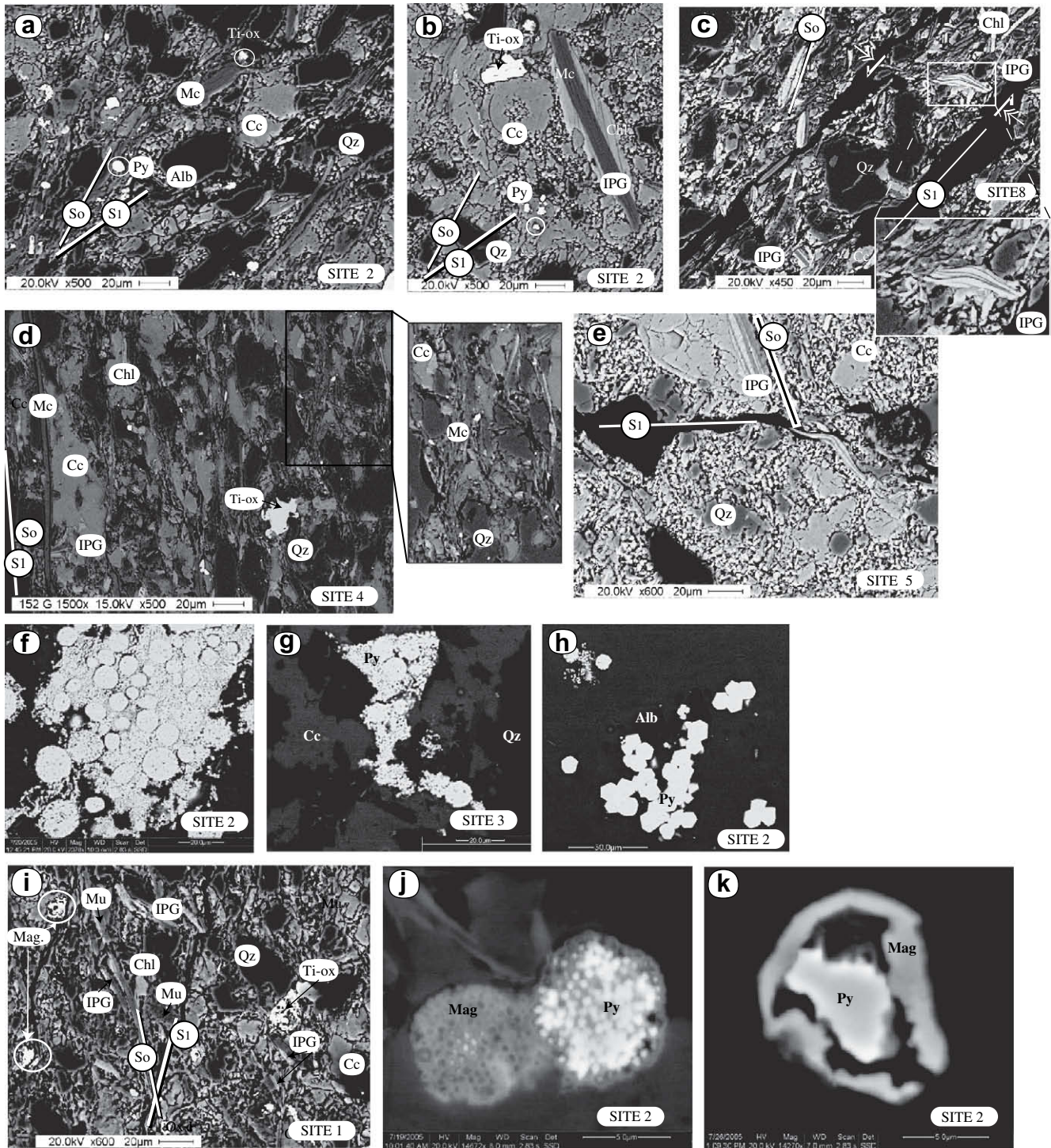
Fig. 6. BSE images showing textural relationships between different mineral constituents of the studied rocks and with respect to bedding (So) and cleavage (S₁) planes (see text). Qz: Quartz; Cc: calcite; Mc: Muscovite; Ch: chlorite; IPG: interleaved phyllosillicate grains; Alb: albite; Py: pyrite; Ti-oxides; Mag: magnetite.

perpendicular to the shortening direction while their K_{min} axes remain perpendicular to bedding (Kissel et al., 1986; Sagnotti and Speranza, 1993; Parés et al., 1999; Parés and van der Pluijm, 2002, 2004; Larrasoaña et al., 2004). The LT-AMS ellipsoids described for the studied rocks therefore suggest a period of layer-parallel shortening in the area (Fig. 9b), which we identified as the one postulated by Teixell et al. (2000). If so, it has to be simultaneous with deposition of the studied sediments, and must therefore be Campanian–Maastrichtian in age. Since the Lakora basement thrust to the north was active since the Santonian, we propose that the

layer-parallel shortening detected by the LT-AMS fabrics is the expression of the strain caused by the Lakora basement thrust in its footwall.

SEM observations show that detrital IPG composed of chlorite/ mica appear occasionally rotated or bent near cleavage planes, and also indicate that white mica crystals occasionally grew authigenically along cleavage planes (Fig. 6). Both of these processes are compatible with a clustering of K_{max} axes around the intersection lineation, but are at odds with the clustering of K_{min} axes around the beding poles. These results suggest that the formation of
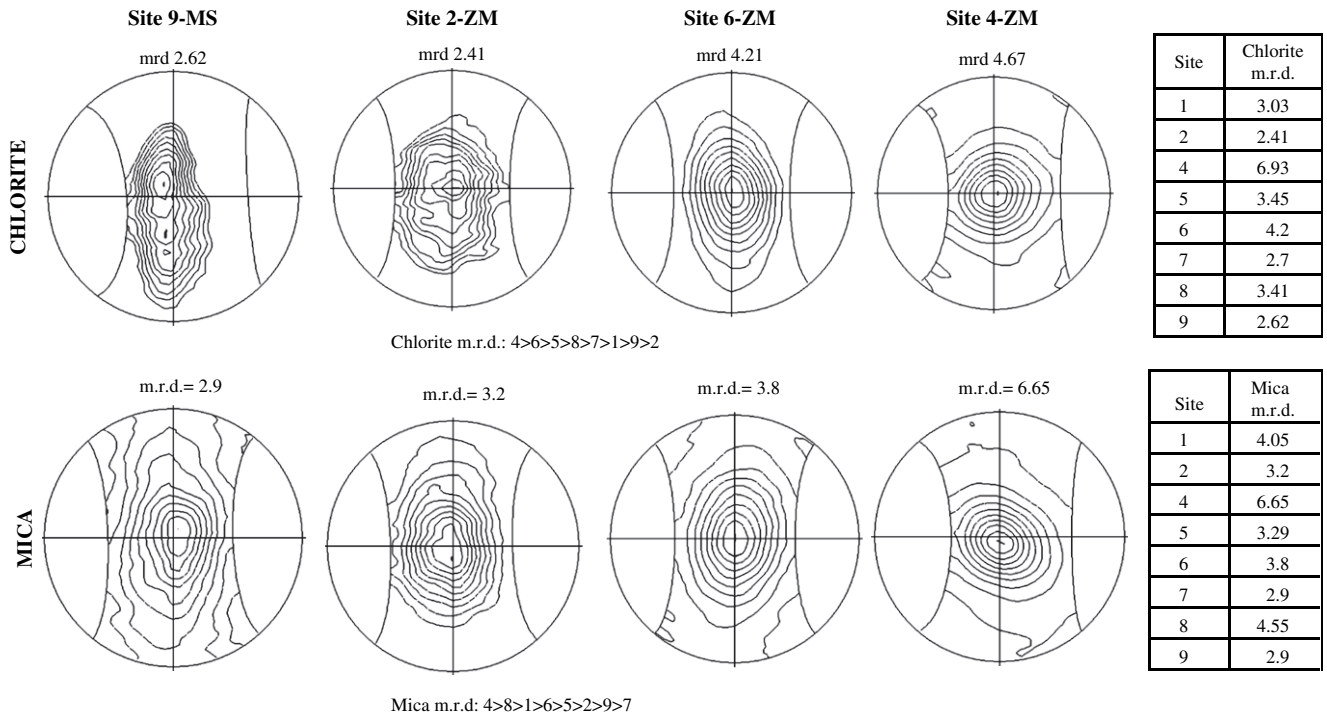
Fig. 7. Equal area, lower-hemisphere projection of XTG data for both mica and chlorite.

cleavage, with its associated rotation of detrital IPG and formation of authigenic white mica did not suffice to overcome the initial phyllosilicate fabric that records the syn-sedimentary layer-parallel shortening. We attribute this circumstance to the fact that the volume of rock constituted by discrete cleavage planes must represent a minor part of the total rock volume (Fig. 9.b).

The AARM ellipsoids also display a homogeneous behavior with respect to structural elements regardless of fabric type (Fig. 4). Thus, their K_{max} axes cluster perpendicular to the intersection lineation, and lie along a NNE–SSW subhorizontal direction but in the case of site 4, where the K_{max} axes cluster subvertical parallel to the stretching lineation measured on the foliation plane. This
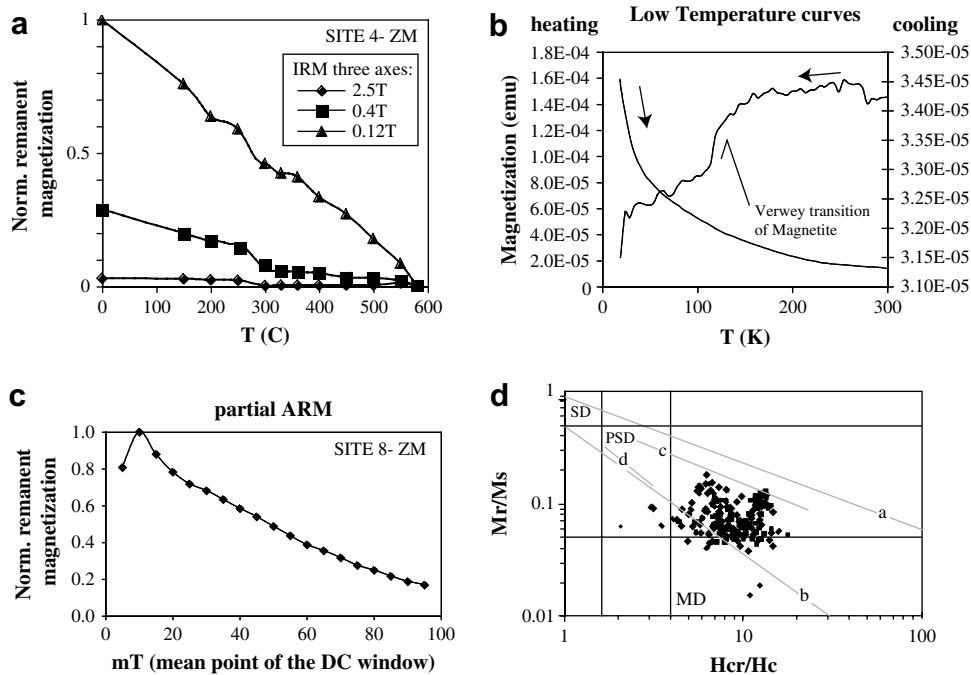

Fig. 8. Rock magnetic results representative for the rocks. (a) Three-component IRM; (b) low-temperature curves; (c) partial anisotropy of the remanent magnetization; and (d) hysteresis results plotted in a Day diagram. Line (a) indicates North American remagnetized limestones (Jackson, 1990); line (b) indicates a mixture of SD and MD grains (Parry, 1982); line (c) indicates remagnetized limestones (Channell and McCabe, 1994; Dinarès-Turell and García-Senz, 2000); and line (d) indicates unremagnetized limestones (Channell and McCabe, 1994; Dinarès-Turell and García-Senz, 2000).
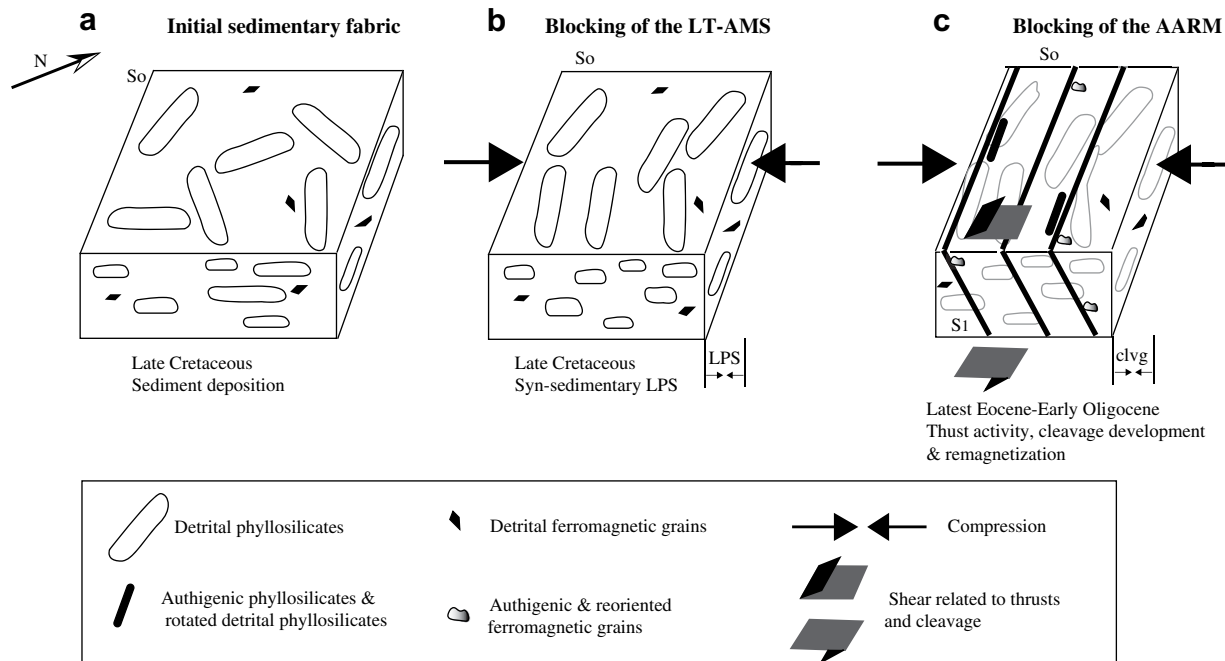
Fig. 9. Sketch showing the evolution of the magnetic subfabrics of the studied rocks in connection with the tectonic history of the Internal Sierras. (a) initial sedimentary fabric characterizing Campanian to Maastrichtian sediment deposition; (b) initial (Campanian to Maastrichtian) tectonic overprint caused by layer-parallel shortening, which affects the orientation of the phyllosilicates and leads to the blocking of the LT-AMS ellipsoids; and (c) subsequent (Late Eocene–Early Oligocene) tectonic overprint caused by thrust activity and cleavage formation, which affects the orientation of authigenic and rotated magnetic grains during the lock in of the remagnetization and blocking of the AARM ellipsoids.

dominant NNE–SSW orientation strikingly coincides with the transport direction measured on thrusts ramps (Teixell et al., 2000). This suggests that the blocking of the AARM ellipsoids occurred during a major period of subhorizontal shear deformation linked to thrusting along the Larra-Monte Perdido thrust system. An alternative possibility is that the AARM ellipsoids were blocked during subhorizontal shear associated to the formation of cleavage at the latest stages of the emplacement of the Gavarnie thrust. The occurrence of a pervasive remagnetization in the studied rocks, which has been linked to formation of cleavage (Oliva-Urcia and Pueyo, 2007; Oliva-Urcia et al., 2008), suggest that the second possibility is more likely because it involves a modification of the remanence properties that might account for the final configuration of the AARM ellipsoids (Fig. 9c).

SEM observations have shown the occurrence of both authigenic magnetite grains dispersed within the rock matrix and of detrital magnetite grains located alongside cleavage planes (Fig. 6). This confirms the proposed mechanism for the origin of the remagnetization, i.e. the liberation and reorientation of previously existing magnetite grains during formation of pressure-solution cleavage (Oliva-Urcia et al., 2008). It also indicates that precipitation of new magnetic phases, which accounts for the wasp-waisted hysteresis loops, might have played a significant role in the acquisition of the remagnetization. Regardless the specific age of the AARM ellipsoids, it appears that their blocking was significantly affected by tectonic deformation, which might have important implications for understanding the paleomagnetic significance of the remagnetization.

6. Conclusions

The RT-AMS fabrics of the studied rocks show a heterogeneous behavior despite the homogeneous lithology and structural setting that characterize the studied sites. Their K_{max} and K_{min} axes do not simultaneously cluster around the intersection lineation and the pole to cleavage, respectively, as has been typically reported for cleaved sedimentary rocks. The measurement of the low-temperature magnetic susceptibility (LT-AMS) and the anisotropy of the anhysteretic remanent magnetization (AARM) have enabled separation of the bulk magnetic fabrics into their paramagnetic and ferrimagnetic components, respectively. LT-AMS ellipsoids show remarkably constant directional properties, with K_{max} axes parallel to the intersection lineation and K_{min} axes parallel to the pole to bedding. These ellipsoids, which result from the preferred orientation of chlorite, mica and IPG grains, reflect a syn-sedimentary (Late Cretaceous) period of layer-parallel shortening in response to tectonic activity along the Lakora thrust located to the North of the studied area. AARM ellipsoids also show remarkably constant orientations, being their K_{max} oriented along a subhorizontal NNE direction that is strikingly coincident with the shortening direction in the studied area. We interpret that the ferrimagnetic ellipsoids respond to subhorizontal shear associated to cleavage formation in the area, a process that did not further alter the paramagnetic subfabrics. Our results reinforce the view that a proper understanding of the structural significance of complex RT-AMS ellipsoids demands its separation into different subfabrics (i.e. paramagnetic and ferrimagnetic), even in cases where the contribution of ferrimagnetic grains might be considered minor.

discussions. We deeply acknowledge the revisions from G.J. Borradaile, which helped to substantially improve the first version of the manuscript. Finally, we acknowledge the helpful handling of the editor R.E. Holdsworth.

Appendix. Supplementary material

Supplementary data associated with this article can be found, in the online version, at doi:10.1016/j.jsg.2008.11.002

References

Aranguren, A., Cuevas, J., Tubía, J.M., 1996. Composite magnetic fabrics from S–C mylonites. J. Struct. Geol. 18 (7), 863–869.

Aubourg, C., Rochette, P., Vialon, P., 1991. Subtle stretching lineation revealed by magnetic fabric of Callovian–Oxfordian black shales (French Alps). Tectonophysics 185, 211–223.

Aubourg, C., Rochette, P., Bergmüller, F., 1995. Composite magnetic fabric in weakly deformed black shales. Phys. Earth Planet. Inter. 87, 267–278.

Aubourg, C., Frizon de Lamotte, D., Poisson, A., Mercier, E., 1997. Magnetic fabrics and oblique ramp-related folding: a case study from the western Taurus (Turkey). J. Struct. Geol. 19 (8), 1111–1120.

Aubourg, C., Rochette, P., Stéphanc, J.-F., Popoff, M., Chabert-Pellinec, C., 1999. The magnetic fabric of weakly deformed Late Jurassic shales from the southern subalpines chains (French Alps): evidence for SW-directed tectonic transport direction. Tectonophysics 307 (1–2), 15–31.

Aubourg, C., Hebert, R., Jolivet, L., Cartayrade, G., 2000. The magnetic fabric of metasediments in a detachment shear zone: the example of Tinos Island (Greece). Tectonophysics 321, 219–236.

Aubourg, C., Robion, P., 2002. Composite ferromagnetic fabrics (magnetite, greigite) measured by AMS and partial AARM in weakly strained sandstones from western Makran, Iran. Geophys. J. Int. 151 (3), 729–737.

Averbuch, O., Frizon de Lamotte, D., Kissel, C., 1992. Magnetic fabric as a structural indicator of the deformation path within a fold-thrust structure: a test case from the Corbieres (NE Pyrenees, France). J. Struct. Geol. 14, 461–474.

Borradaile, G.J., 1987. Anisotropy of magnetic susceptibility: rock composition versus strain. Tectonophysics 138, 327–329.

Borradaile, G.J., Tarling, D.H., 1981. The influence of deformation mechanisms on magnetic fabrics in weakly deformed rocks. Tectonophysics 77, 151–168.

Borradaile, G.J., Tarling, D.H., 1984. Strain partitioning and magnetic fabrics in particulate flow. Can. J. Earth Sci. 21, 694–697.

Borradaile, G.J., Henry, B., 1997. Tectonic applications of magnetic susceptibility and its anisotropy. Earth Sci. Rev. 42, 49–93.

Borradaile, G.J., Lagroix, F., King, D., 1998. Tilting and transpression of an Archaean anorthosite in northern Ontario. Tectonophysics 293 (3-4), 239–254.

Borradaile, G.J., Werner, T., Lagroix, F., 1999. Magnetic fabrics and anisotropy-controlled thrusting in the Kapuskasing Structural Zone, Canada. Tectonophysics 302, 241–256.

Borradaile, G.J., Jackson, M., 2004. Anisotropy of magnetic susceptibility (AMS): magnetic petrofabrics of deformed rocks. In: Martín-Hernández, F., Lüneburg, C.M., Aubourg, C., Jackson, M. (Eds.), Magnetic Fabric, Methods and Applications. Geological Society Special Publication, 238, pp. 299–360.

Channell, J.E.T., McCabe, C., 1994. Comparison of magnetic hysteresis parameters of unremagnetized and remagnetized limestones. J. Geophys. Res. 99, 4613–4623.

Choukroune, P., 1976. Structure et évolution tectonique de la zone nord-pyrénéene: Analyse de la déformation dans une portion de la chaîne à schistosité sub-verticale. Mem. Soc. Geol. Fra. 127, 1–116.

Choukroune, P., Séguret, M., 1973. Carte Structurale des Pyrénées. ELF-ERAP. Mission France. Boussens.

Day, R., Fuller, M., Schmidt, V.A., 1977. Hysteresis properties of titanomagnetites: grain-size and compositional dependence. Phys. Earth Planet. Inter. 13, 260–267.

Dinarès-Turell, J., García-Senz, J., 2000. Remagnetization of Lower Cretaceous limestones from the southern Pyrenees and relation to the Iberian plate geodynamic evolution. J. Geophys. Res. 105B, 19405–19418.

Durney, D.W., Kisch, H., 1994. A field classification and intensity scale for first-generation cleavages. J. Aust. Geol. Geophys. 15, 257–295.

Evans, M.A., Elmore, R.D., 2006. Fluid control of localized mineral domains in limestone pressure solution structures. J. Struct. Geol. 28, 284–301.

Ferré, E.C., Améglio, L., 2000. Preserved magnetic fabrics vs. annealed microstructures in the syntectonic recrystallised George granite, South Africa. J. Struct. Geol. 22 (8), 1199–1219.

Girdler, R.W., 1961. The measurement and computation of anisotropy of magnetic susceptibility in rocks. Geophys. J.R. Astron. Soc. 5, 34–44.

Hirt, A.M., Julivert, M., Soldevila, J., 2000. Magnetic fabric and deformation in the Navia-Alto Sil slate belt, northwestern Spain. Tectonophysics 320 (1), 1–16.

Hirt, A.M., Schmidt, V., Almqvist, B.S.G., 2004. Understanding magnetic fabrics. Geotectonic Res. 95 (1), 65–67.

Ho, N-Ch, Peacor, D.R., van der Pluijm, B.A., 1994. Reorientation mechanisms of phyllosilicates in the mudstone-to-slate transition at Lehigh Gap, Pennsylvania. J. Struct. Geol. 17 (3), 345–356.

Holl, J.E., Anastasio, D.J., 1995. Cleavage development within foreland fold and thrust belt, southern Pyrenees, Spain. J. Struct. Geol. 17 (3), 357–369.

Housen, B.A., van der Pluijm, B., 1991. Slaty cleavage development and magnetic anisotropy fabrics. J. Geophys. Res. 96, 9937–9946.

Housen, B.A., Richter, C., van der Pluijm, B.A., 1993a. Composite magnetic anisotropy fabrics: experiments, numerical models, and implications for the quantification of rock fabrics. Tectonophysics 220, 1–12.

Housen, B.A., van der Pluijm, B.A., van der Voo, R., 1993b. Magnetite dissolution and neocrystallization during cleavage formation; paleomagnetic study of the Martinsburg Formation, Lehigh Gap, Pennsylvania. J. Geophys. Res. 98, 13799–13813.

Hrouda, F., 1982. Magnetic anisotropy of rocks and its application in geology and geophysics. Geophys. Surv. 5, 37–82.

Jackson, M., 1990. Diagenetic sources of stable remanence in remagnetized Paleozoic cratonic carbonates: a rock magnetic study. J. Geophys. Res. 95, 2753–2761.

Jackson, M., Gruber, W., Marvin, J., Banerjee, K., 1988. Partial anhysteretic remanence and its anisotropy: applications and grainsize-dependance. Geophys. Res. Lett. 15 (5), 440–443.

Jelínek, V., 1981. Characterization of the magnetic fabric of rocks. Tectonophysics 79, 63–70.

Kelso, P.R., Tikoff, B., Jackson, M., Sun, W., 2002. A new method for the separation of paramagnetic and ferromagnetic susceptibility anisotropy using low field and high field methods. Geophys. J. Int. 151 (2), 345–359.

Kissel, C., Barrier, E., Laj, C., Lee, T.Q., 1986. Magnetic fabric in 'undeformed' marine clays from compressional zones. Tectonics 5, 769–781.

Kligfield, R., Owens, W.H., Lowrie, W., 1981. Magnetic susceptibility anisotropy, strain and progressive deformation in Permian sediments from the Maritime Alps (France). Earth Planet. Sci. Lett. 55, 181–189.

Labaume, P., Séguret, M., Seyve, C., 1985. Evolution of a turbiditic foreland basin an analogy with an accretionary prism: example of the Eocene South-Pyrenean basin. Tectonics 4 (7), 661–685.

Lamarche, G., Rochette, P., 1987. Microstructural analysis and origin of lineations in the magnetic fabric of some Alpine slates. Tectonophysics 139 (3–4), 285–293.

Larrasoaña, J.C., Pueyo, E.L., Parés, J.M., 2004. An integrated AMS structural, paleo- and rock-magnetic study of the Eocene marine marls from the Jaca-Pamplona basin (Pyrenees, N Spain); new insights into the timing of magnetic fabric acquisition in weakly deformed mudrocks. In: Martín-Hernández, F., Lüneburg, C.M., Aubourg, C., Jackson, M. (Eds.), Magnetic Fabric, Methods and Applications. Geological Society Special Publication, 238, pp. 127–143.

Lewchuk, M.T., Evans, M., Elmore, R.D., 2003. Synfolding remagnetization and deformation: results from Paleozoic sedimentary rocks in West Virginia. Geophys. J. Int. 152, 266–279.

Lowrie, W., 1990. Identification of ferromagnetic minerals in a rock by coercivity and unblocking temperature properties. Geophys. Res. Lett. 17 (2), 159–162.

Martín-Chivelet, J., Berástegui, X., Caus, E., Puig, C., 2002. Cretaceous. In: Gibbons, W., Moreno, T. (Eds.), Geology of Spain. Geological Society, London, pp. 255–292.

Martín-Hernández, F., Ferré, E.C., 2007. Separation of paramagnetic and ferromagnetic anisotropies: a review. J. Geophys. Res. 112, doi:10.1029/2006JB004340.

McCabe, C., Jackson, M., Ellwood, B.B., 1985. Magnetic anisotropy in the Trenton limestone: results of a new technique, anisotropy of anhysteretic susceptibility. Geophys. Res. Lett. 12, 333–336.

McCaig, A.M., Tritlla, J., Banks, D.A., 2000. Fluid mixing and recycling during Pyrenean thrusting: evidence from fluid inclusion halogen ratios. Geochim. Cosmochim. Acta 64 (19), 3395–3412.

Millán, H., 1996. Estructura y cinemática del frente de cabalgamiento surpirenaico en las Sierras Exteriores Aragonesas. Tesis Doctoral. Universidad de Zaragoza, 330 pp.

Muñoz, J.A., 1992. Evolution of a continental collision belt: ECORS-Pyrenees crustal balanced section. In: McClay, K.R. (Ed.), Thrust Tectonics. Chapman and Hall, London, pp. 235–246.

Nagata, T., 1961. Rock Magnetism, second ed. Maruzen, Tokyo, 350 pp.

Oliva-Urcia, B., Pueyo, E.L., 2007. Rotational basement kinematics deduced from remagnetized cover rocks (Internal Sierras, southwestern Pyrenees). Tectonics 26, TC4014, doi:10.1029/2006TC001955.

Oliva-Urcia, B., Pueyo, E.L., Larrasoaña, J.C., 2008. Magnetic reorientation induced by pressure solution: a potential mechanism for orogenic-scale. Earth Planet. Sci. Lett. 265, 525–534.

Parés, J.M., Dinarés-Turell, J., 1993. Magnetic fabric in two sedimentary rock types from the Southern Pyrenees. J. Geomag. Geoelectr. 45, 193–205.

Parés, J.M., van der Pluijm, B.A., Dinarés-Turell, J., 1999. Evolution of magnetic fabrics during incipient deformation of mudrocks (Pyrenees, northern Spain). Tectonophysics 307, 1–14.

Parés, J.M., van der Pluijm, B., 2002. Evaluating magnetic lineations (AMS) in deformed rocks. Tectonophysics 350, 283–298.

Parés, J.M., van der Pluijm, B.A., 2004. Correlating magnetic fabrics with finite strain: comparing results from mudrocks in the Variscan and Appalachian Orogens. Geologica Acta 2 (3), 213–220.

Parry, L.G., 1982. Magnetization of inmobilized particle dispersions with two distinct particle sizes. Phys. Earth Planet. Inter. 28, 230–241.

van der Pluijm, B.A., Ho, N.-C., Peacor, D., 1994. High-resolution X-ray texture goniometry. J. Struct. Geol. 16 (7), 1029–1032.

Rathore, J.S., 1985. Some magnetic fabric characteristics of sheared zones. J. Geodynamics 2 (2–3), 291–301.

Robion, P., Averbuch, O., Sintubin, M., 1999. Fabric development and metamorphic evolution of lower Palaeozoic slaty rocks from the Rocroi massif (French–

Belgian Ardennes): new constraints from magnetic fabrics, phyllosilicate preferred orientation and illite crystallinity data. Tectonophysics 309 (1–4), 257–273.

Rochette, P., 1987. Magnetic susceptibility of the rock matrix related to magnetic fabric studies. J. Struct. Geol. 9, 1015–1020.

Sagnotti, L., Speranza, E., 1993. Magnetic fabric analysis of the Plio-Pleistocene clayey units of the Sant'Arcangelo basin, southern Italy. Phys. Earth Planet. Inter. 77, 165–176.

Séguret, M., 1972. Etude tectonique des nappes de series décollées de la partie centrale du versant sud des Pyrénées. Caractère synsédimentaire, rôle de la compression et de la gravité. Thèse Doct. Publ. USTELA, Série Géol, Montpellier, 155 pp.

Singh, J., Sanderson, D.J., Tarling, D.H., 1975. The magnetic susceptibility anisotropy of deformed rocks from North Cornwall, England. Tectonophysics 27, 141–153.

Suk, D., Peacor, D.R., Van der Voo, R., 1990. Replacement of pyrite framboids by magnetite in limestone and implications for paleomagnetism. Nature 345, 611–613.

Suk, D., Van der Voo, R., Peacor, D.R., Lohmann, K., 1993. Late Paleozoic remagnetization and its carrier in the Trenton and Black River carbonates from the Michigan Basin. J. Geol. 101 (6), 795–808.

Sun, W., Jackson, M., Craddock, J.P., 1993. Relationship between remagnetization, magnetic fabric and deformation in Paleozoic carbonates. Tectonophysics 221, 361–366.

Teixell, A., 1992. Estructura alpina en la transversal de la terminación occidental de la Zona Axial pirenaica. Tesis doctoral, Universitat de Barcelona, 252 pp.

Teixell, A., 1996. The Ansó transect of the southern Pyrenees: basement and cover thrust geometries. J. Geophys. Res. 102, 20325–20342.

Teixell, A., 1998. Crustal structure and orogenic material budget in the west central Pyrenees. Tectonics 17 (3), 395–406.

Teixell, A., Durney, D.W., Arboleya, M.L., 2000. Stress and fluid control on decollement within competent limestone. J. Struct. Geol. 22, 349–371.

Travé, A., Labaume, P., Calvet, F., Soler, A., 1997. Sediment dewatering and pore fluid migration along thrust faults in a foreland basin inferred from isotopic and elemental geochemical analyses (Eocene southern Pyrenees, Spain). Tectonophysics 282, 375–398.

Veblen, D.R., Ferry, J.M., 1983. A TEM study of the biotite–chlorite reaction and comparison with petrological observations. American Mineralogist 68, 1160–1168.

Weil, A.B., van der Voo, R., 2002. Insights into the mechanism for orogen-related carbonate remagetization from growth of authigenic Fe-oxide: A scanning electron microscopy and rock magnetic study of Devonian carbonates from northern Spain. J. Geophys. Res. 107B4, doi:10.1029/2001JB000200.

Wenk, H.R., 1985. Measurements of pole figures. In: Wenk, H.R. (Ed.), Preferred Orientation in Deformed Metals and Rocks: an Introduction to Modern Texture Analyses. Academic Press, New York.

Zegers, T.E., Dekkers, M.J., Bailly, S., 2003. Late Carboniferous to Permian remagnetization of Devonian limestones in the Ardennes: role of temperature, fluids, and deformation. J. Geophys. Res. 108 (B7), 2357–2376.